A tetranuclear Mn-diamond core complex as a functional mimic of both catechol oxidase and phenoxazinone synthase enzymes

Rakesh Kumar, Rahul Keshri, Koushik Prodhan, Kanchan Shaikh, and Apparao Draksharapu*

Southern Laboratories-208A, Department of Chemistry, Indian Institute of Technology, Kanpur – 208016, India.
Email: appud@iitk.ac.in

Experimental Section:

X-ray crystallography

Single-crystal of suitable dimensions was used for data collection. Diffraction intensities were collected on a Bruker D8 Venture Duo X-ray diffractometer[1] and software suite CCD diffractometer, with graphite-monochromated Mo Kα (0.71073 Å) radiation at 100 K. Data were corrected for Lorentz and polarization effects; empirical absorption corrections (SADABS v 2.10) were applied. Using Olex2,[2] the structures were solved by ShelXT[3] structure solution program using Intrinsic Phasing and refined with the ShelXL[4] refinement package using Least Squares minimization. The non-hydrogen atoms were refined anisotropically, whereas the H atoms fixed to their geometrically ideal positions were refined isotropically. CCDC **2182342** contains the supplementary crystallographic data for **1**. This data can be obtained free of charge from the Cambridge Crystallographic Data Centre via www.ccdc.cam.ac.uk.

Synthesis of Mn Dimer, $[Mn^{II}_2(HPTP^*)]^{3+}$ (3):

To a 2 mL solution of 1,3-bis(bis((4-methoxy-3,5-dimethylpyridin-2-yl)methyl)amino)propan-2-ol (HPTP*H) ligand (105 mg, 0.15 mmol) in acetonitrile, a 2 mL CH_3CN solution of $[Mn^{II}(H_2O)](ClO_4)_2$ (110 mg, 0.30 mmol) was added dropwise with stirring in nitrogen filled glove box. The reaction mixture was stirred of 3 h at room temperature. Excess diethyl ether was poured in the reaction mixture and decanted. The obtained off white solid of **3** washed thrice with Et_2O (3 X 30 mL). UV-Vis absorption spectrum of this complex showed band at 263 nm with ε = 14400 $M^{-1}cm^{-1}$ (Figure S22A). ESI-MS of the complex giving m/z = 929.20 and 993.18, for the formulation $[Mn_2(HPTP^*)(Cl)(ClO_4)]^+$ and $[Mn_2(HPTP^*)(ClO_4)_2]^+$, respectively (Figure S22B). Solution state EPR also confirms the presence of Mn in +2 oxidation state (Figure S22C). However, our efforts to recrystallize this complex were unsuccessful.

Synthesis of $[Mn_4(tpdp)_2(O)_2(H_2O)_4](ClO_4)_5\cdot 4H_2O$ (4):

Synthesis of **4** was carried out as reported procedure by *Akira et. al*.[5] Htpdp is 1,3-bis[bis(2-pyridylmethyl)amino]-2-propanol.

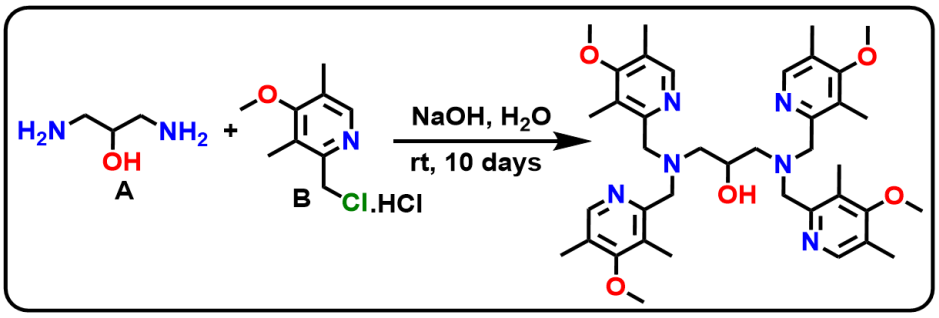

Scheme S1: Synthetic procedure for HPTP*H ligand.

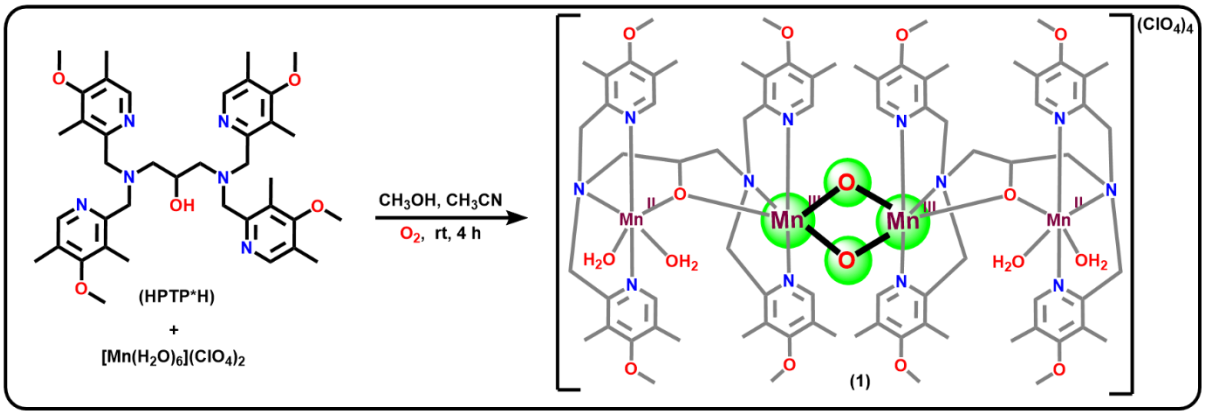

Scheme S2: Synthetic procedure for **1**.

Synthesis of *N,N,N',N'*-tetrakis(2-quinolylmethyl)-2-hydroxy-1,3-propanediamine (Htqhpn): Ligand synthesis was carried out as reported procedure by *Mikata et. al*.[6]

^{1}H NMR (400 MHz, $CDCl_3$): δ 8.02 (d, 4H), 7.92 (d, 4H), 7.69 (d, 4H), 7.66-7.62 (m, 4H), 7.48-7.44 (m, 8H), 4.16 (m, 9H) 2.83 (m, 4H). ^{13}C NMR (100 MHz, $CDCl_3$): δ 159.06, 147.20,136.75, 129.67, 128.77, 127.59, 127.38, 126.40, 121.18, 67.20, 61.40, 59.22 ppm.

Synthesis of $[Mn_4(tqhpn)_2(\mu\text{-}O)_2(H_2O)_2(DMF)_2]\cdot(ClO_4)_4\cdot 4H_2O$ ($2\cdot 4H_2O$).2: Synthesis of **2** was carried out as reported procedure by *Mikata et. al*.[6]

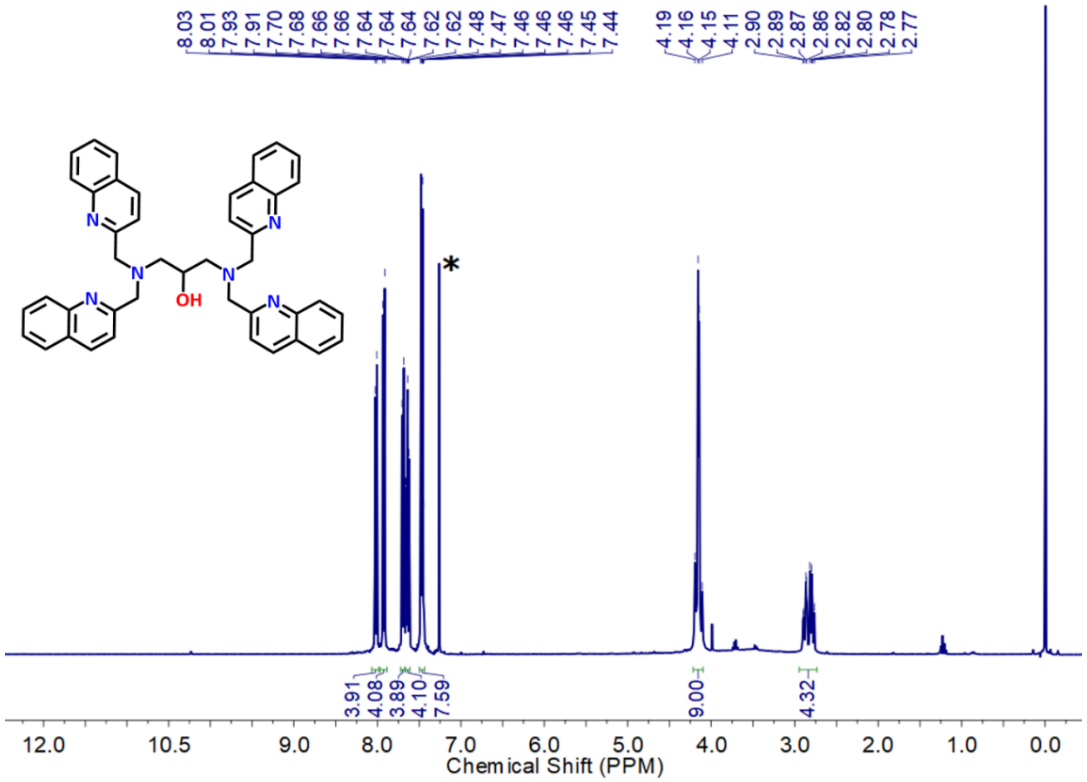

Figure S1: ^{1}H NMR spectrum of *N,N,N',N'*-tetrakis(2-quinolylmethyl)-2-hydroxy-1,3-propanediamine (Htqhpn) in $CDCl_3$ at 400 MHz. (*$CDCl_3$ residual peak)

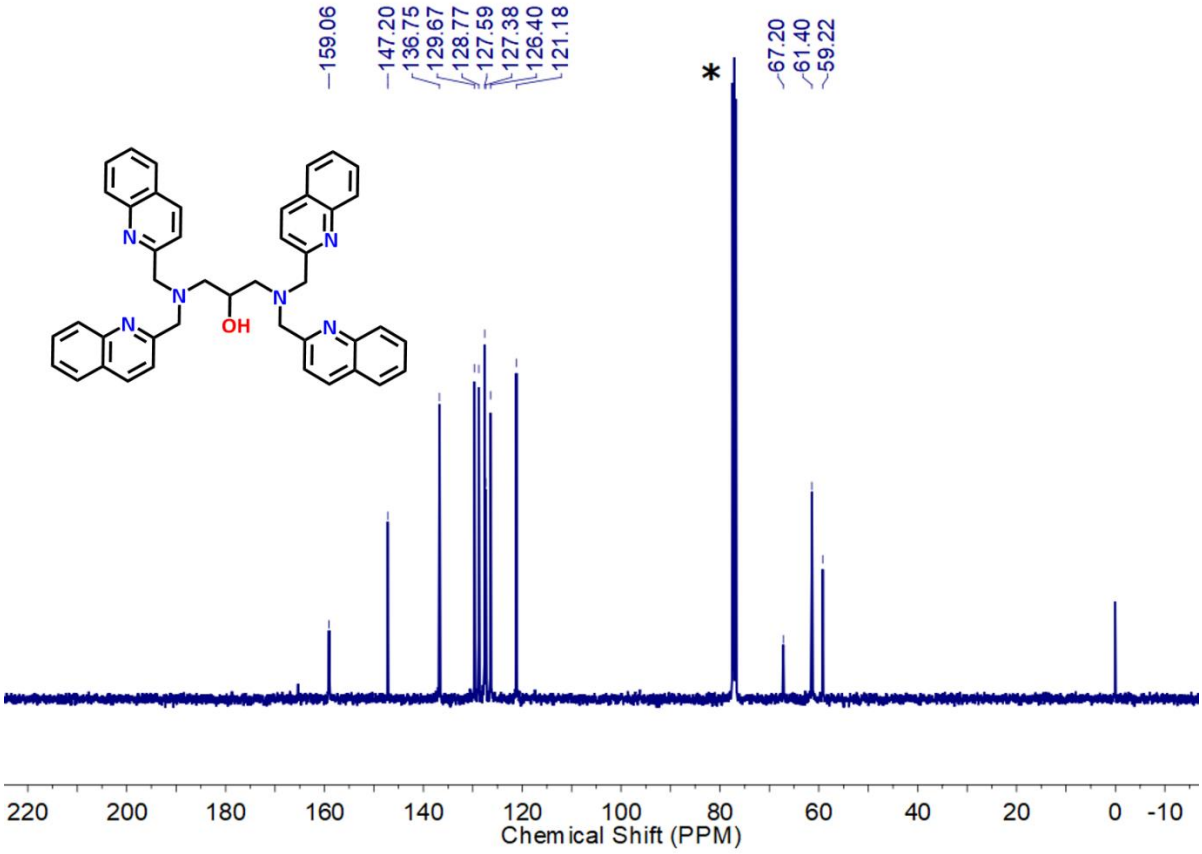

Figure S2: ^{13}C NMR spectrum of *N,N,N',N'*-tetrakis(2-quinolylmethyl)-2-hydroxy-1,3-propanediamine (Htqhpn) in $CDCl_3$ at 100 MHz. (*$CDCl_3$ residual peak)

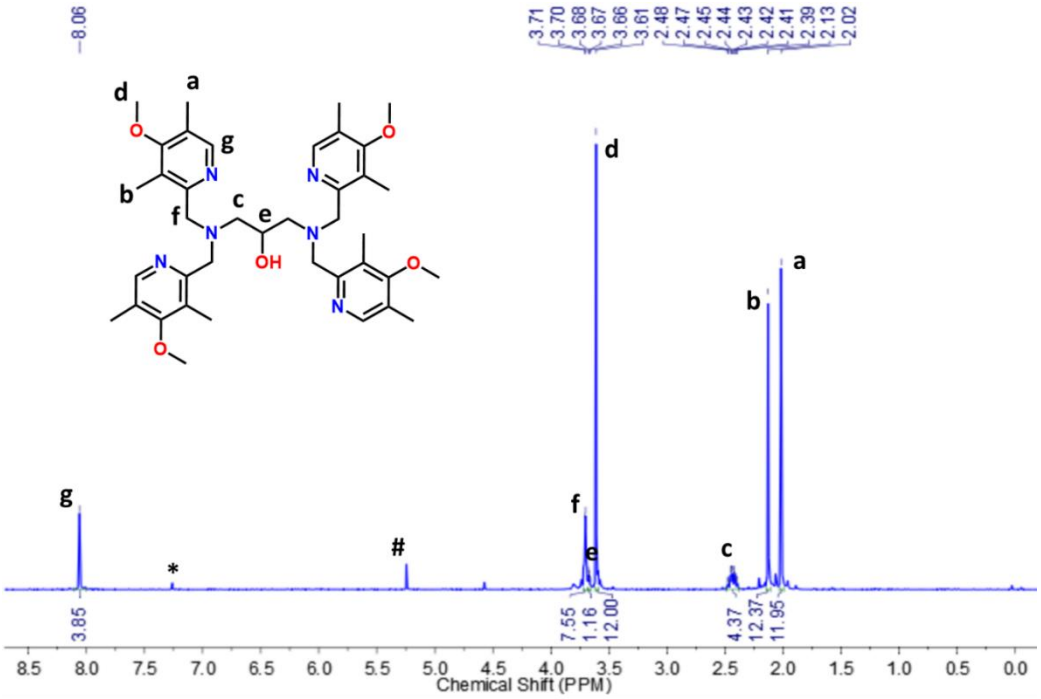

Figure S3: ^{1}H NMR spectrum of 1,3-bis(bis((4-methoxy-3,5-dimethylpyridin-2-yl)methyl)amino)propan-2-ol (HPTP*H) in $CDCl_3$ at 500 MHz. (*$CDCl_3$ residual peak, # peak for dichloromethane solvent)

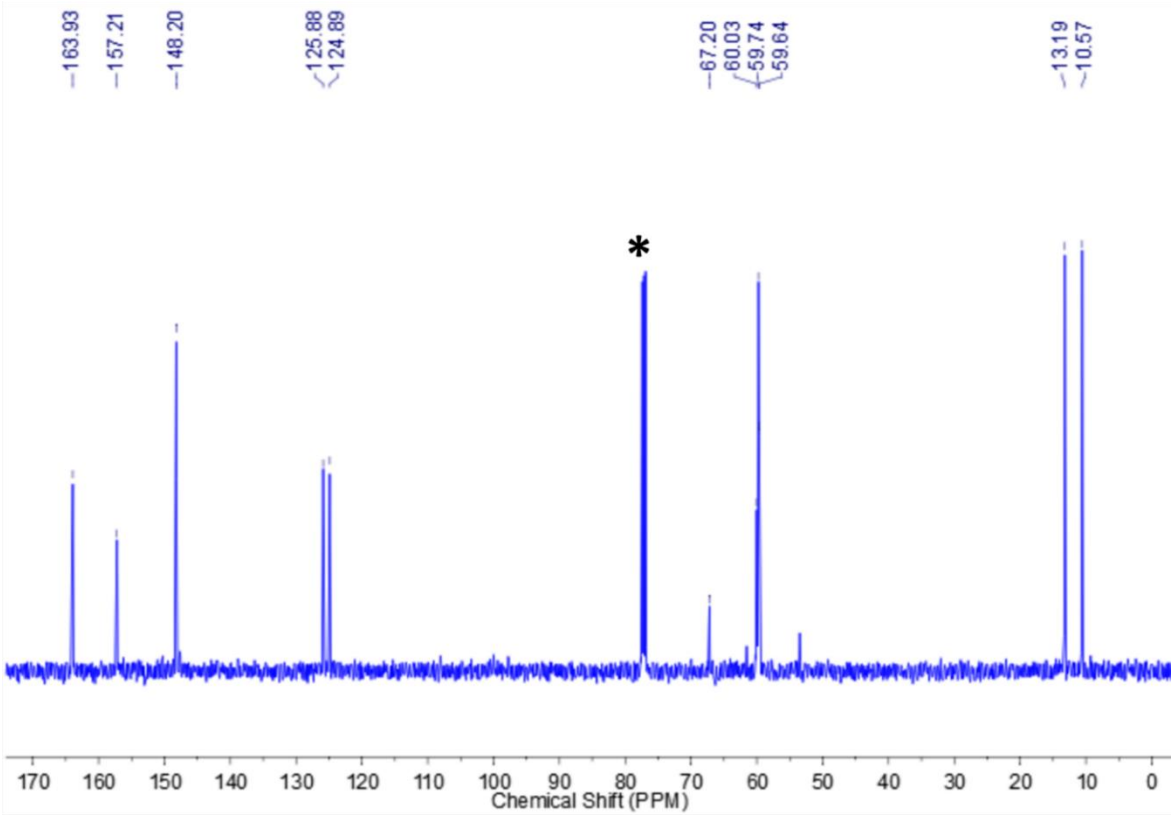

Figure S4: ^{13}C NMR spectrum of 1,3-bis(bis((4-methoxy-3,5-dimethylpyridin-2-yl)methyl)amino)propan-2-ol (HPTP*H) in $CDCl_3$ at 125 MHz. (*$CDCl_3$ residual peak)

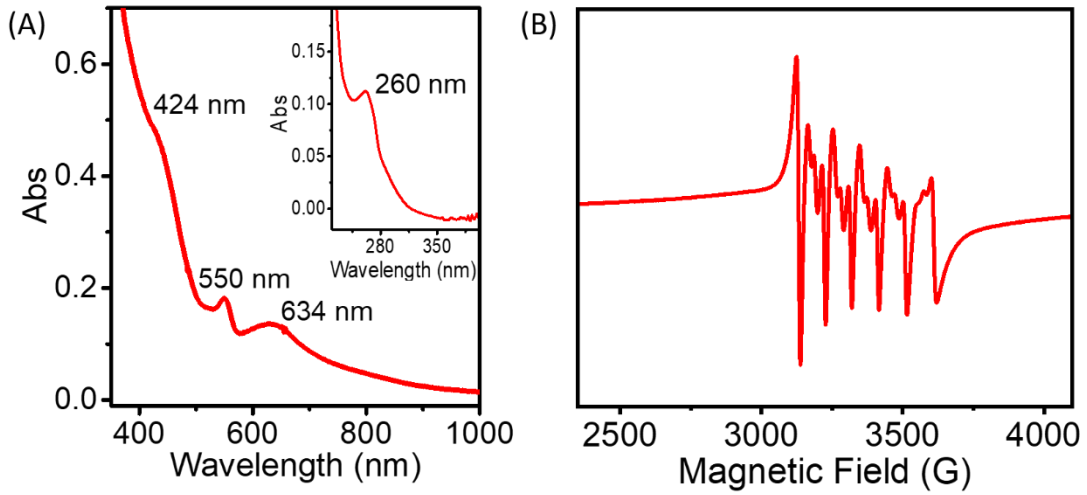

Figure S5: (A) UV-Vis absorption spectrum of 0.25 mM **1** in CH_3CN at room temperature. Inset: UV-Vis absorption spectrum of 5 µM **1** in CH_3CN. (B) X-band EPR spectrum of **1** (in MeOH with a few drops of toluene) measured at 120 K; modulation amplitude 1.98 G, modulation frequency 100 kHz, and microwave frequency 9.466 GHz.

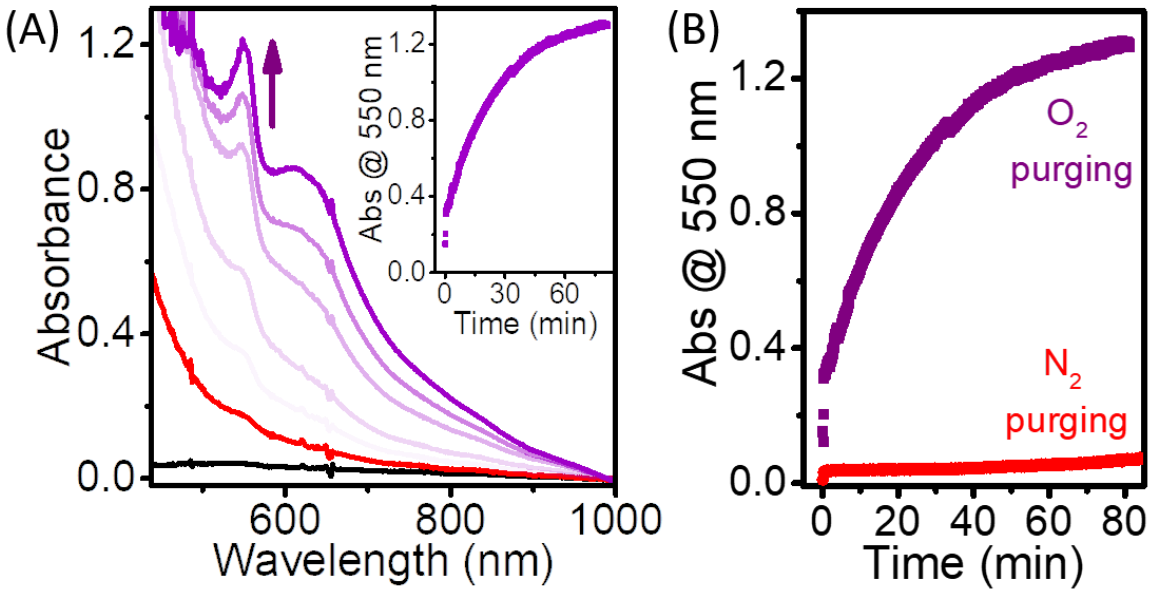

Figure S6. (A) Formation of **1** followed by UV-Vis absorption spectroscopy upon the reaction of HPTP*H (red) with $[Mn^{II}(H_2O)_6](ClO_4)_2$ (black) in CH_3CN at room temperature with dioxygen purging. Inset: The corresponding change in the absorption at 550 nm. (B) Changes observed at 550 nm over time in the presence (purple) and absence of (red) dioxygen.

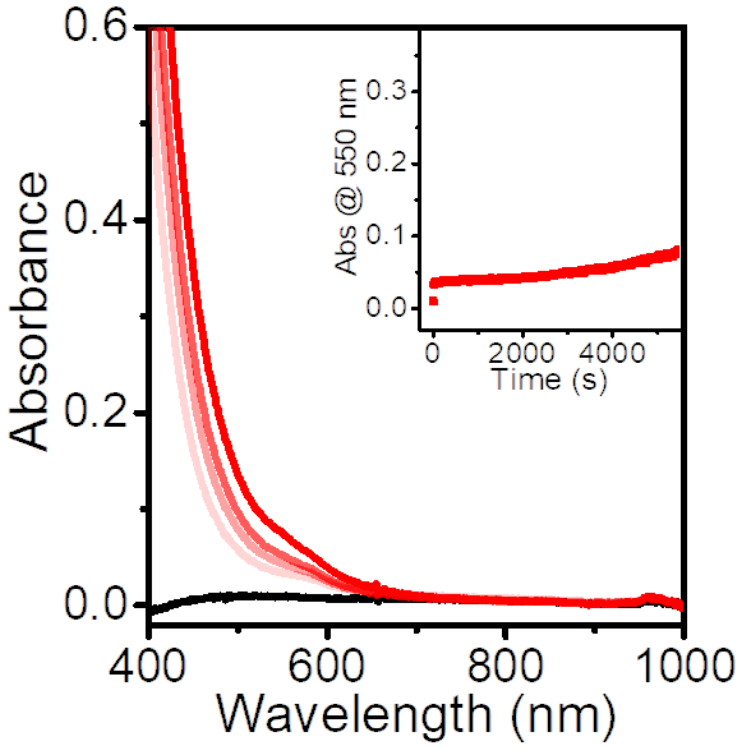

Figure S7. UV-Vis absorption spectral changes observed upon adding HPTP*H to $[Mn^{II}(H_2O)_6](ClO_4)_2$ (black) in CH_3CN at room temperature with N_2 purging. Inset: The corresponding change in the absorption at 550 nm over time.

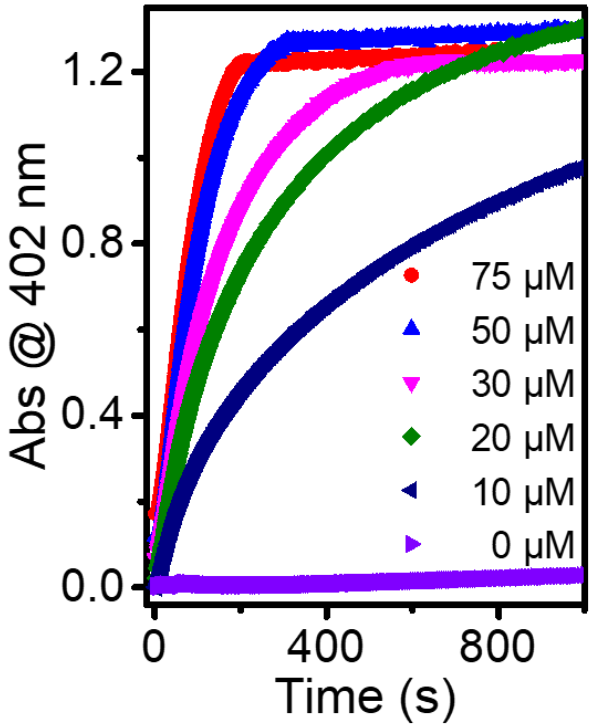

Figure S8: UV-Vis absorption changes observed at 402 nm with time during the reaction of 1 mM 3,5-DTBC with **1** at various concentrations 75 µM (red), 50 µM (blue), 30 µM (magenta), 20 µM (green), 10 µM (dark blue) and 0 µM (purple) in acetonitrile.

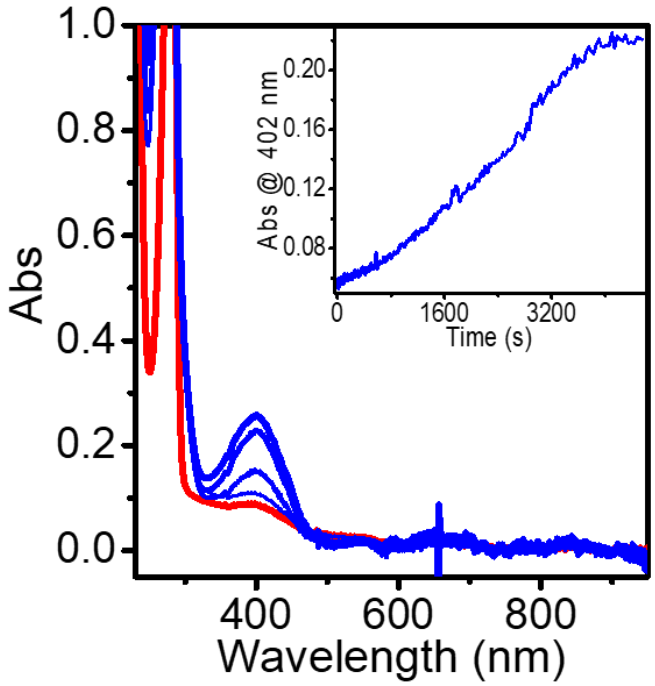

Figure S9: Time-dependent UV-Vis absorption spectral changes upon the reaction of 1 mM 3,5-DTBC with **1** (0.03 mM) in CH_3CN under nitrogen atmosphere. Inset: The corresponding changes in the absorption at 402 nm over time in seconds.

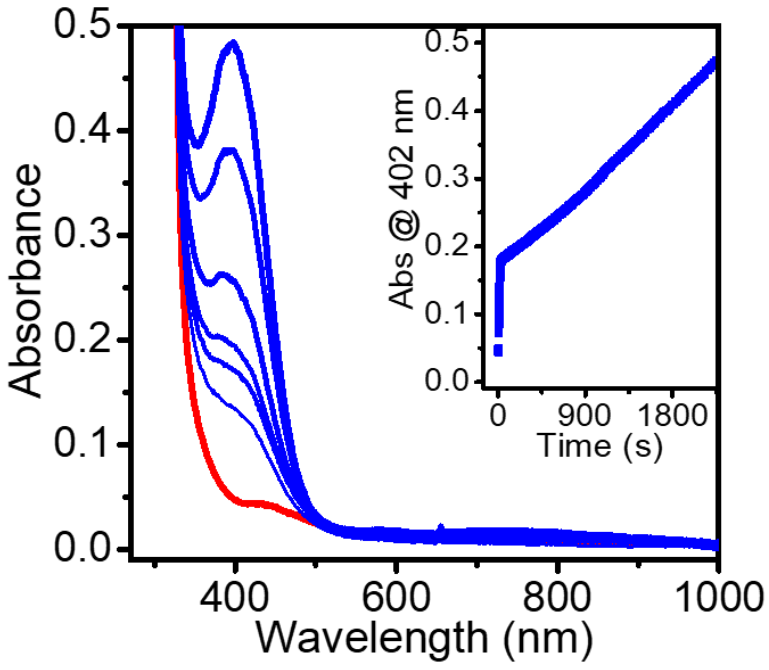

Figure S10: Time-dependent UV-Vis absorption spectral changes upon the reaction of 1 mM 3,5-DTBC with **2** (0.10 mM) in CH_3CN under open air atmosphere. Inset: The corresponding changes in the absorption at 402 nm over time in seconds. *Reaction condition:* Stock of **2** (4 mM in DMF), 3,5 DTBC (100 mM in CH_3CN) prepared. To a 2 mL CH_3CN in a cuvette 3,5-DTBC (20 µL, 100 mM) and **2** (4 mM, 15 µL) were added.

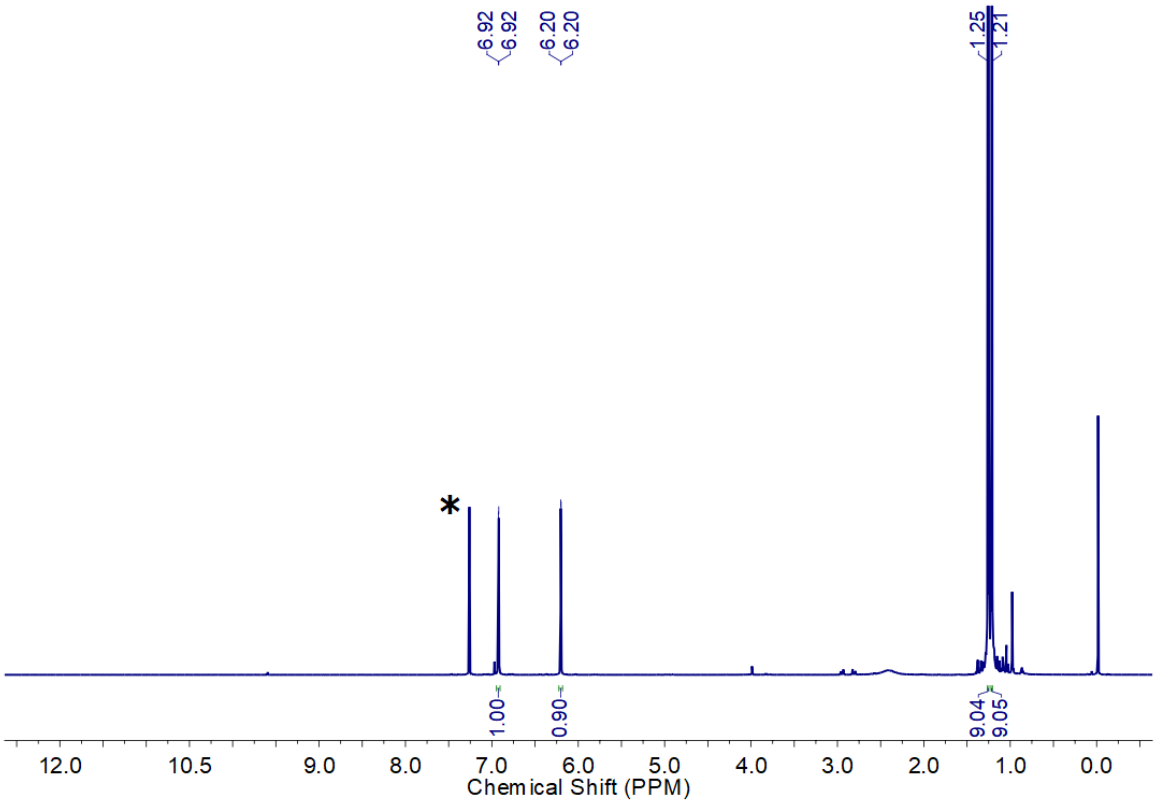

Figure S11: ^{1}H NMR of 3,5-DTBQ. (*$CDCl_3$ residual peak)

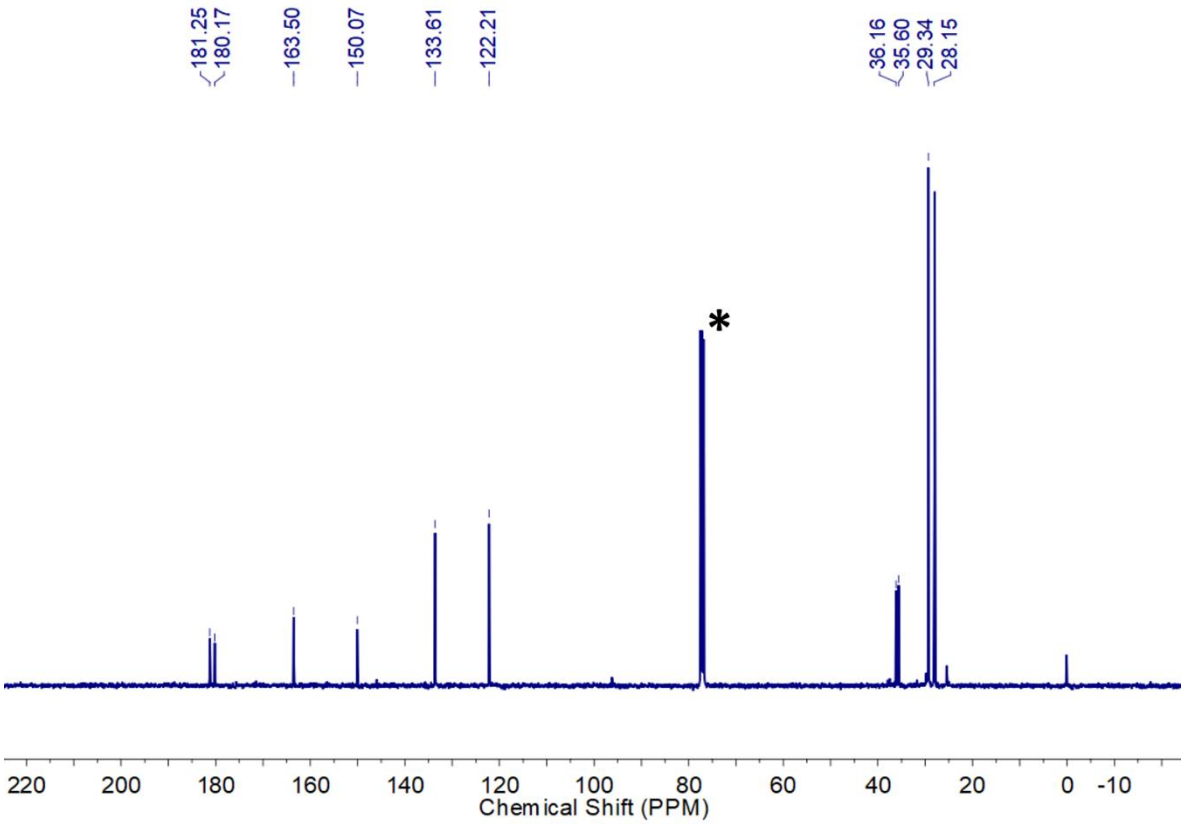

Figure S12: ^{13}C NMR of 3,5-DTBQ. (*$CDCl_3$ residual peak)

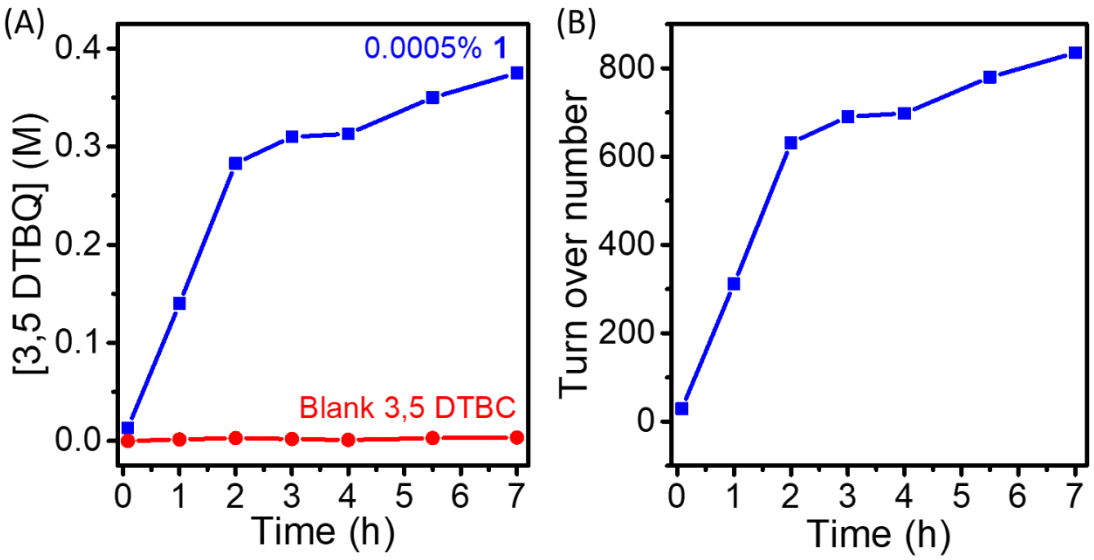

Figure S13: Reaction of 3,5-DTBC with **1** in CH_3CN under open air atmosphere monitored using UV-Vis absorption spectroscopy. (A) Plot of concentration of 3,5-DTBQ (in molar) vs. time (in hours). (Blue) 0.0005% catalyst **1** loading, (Red) in absence of catalyst **1**. (B) Plot of turn over number vs. time (in hours) of the reaction conducted in the aerobic conditions.

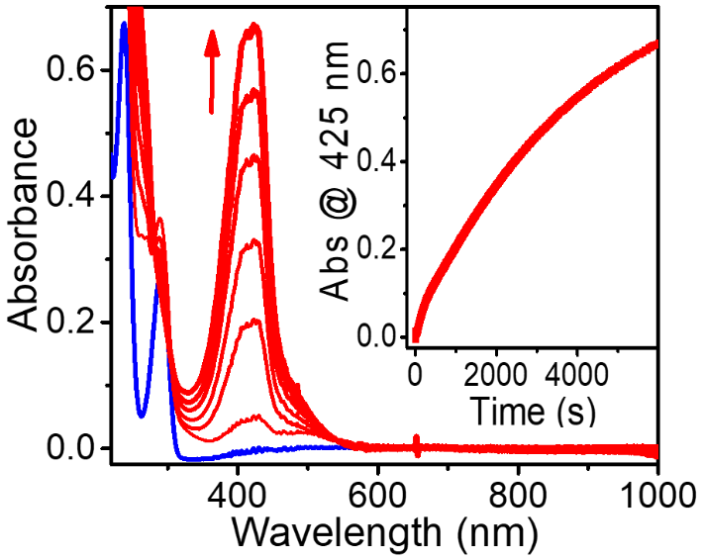

Figure S14. Time-dependent UV-Vis absorption spectral changes upon the reaction of **1** (10 μM) with 0.1 mM 2-aminophenol in CH_3CN in open air atmosphere. Inset: The corresponding changes in the absorption at 425 nm over time in seconds.

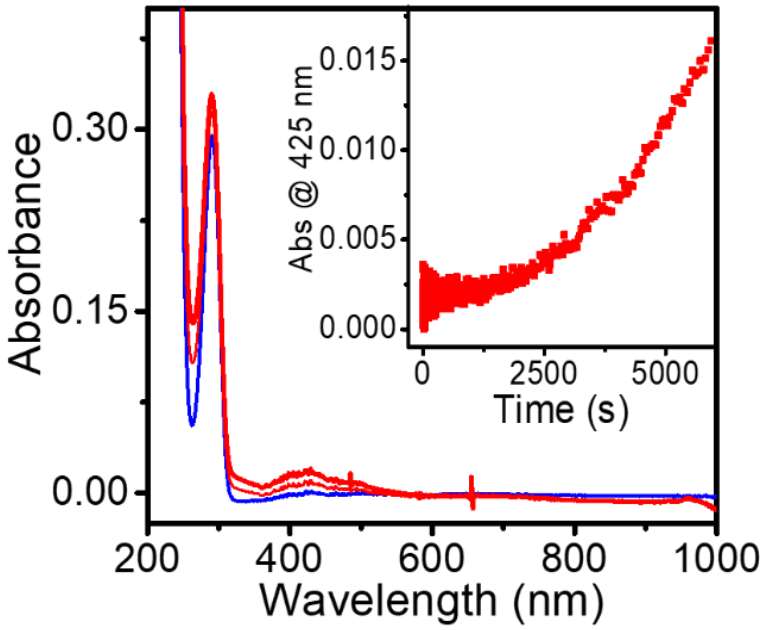

Figure S15. Time-dependent UV-Vis absorption spectral changes upon purging O_2 to 0.1 mM 2-aminophenol in CH_3CN. Inset: Corresponding changes in the absorption at 425 nm over time in seconds.

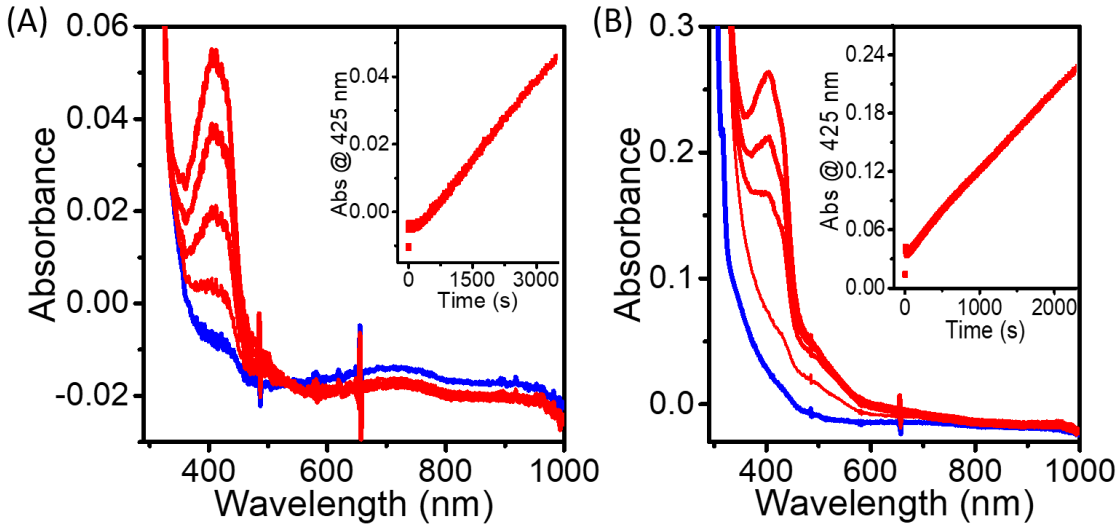

Figure S16. Time-dependent UV-Vis absorption spectral changes upon (A) the reaction of 0.01 mM **2** with 0.1 mM 2-aminophenol under constant purging of O_2 in CH_3CN. Inset: The corresponding changes in the absorption at 425 nm over time in seconds. *Reaction condition:* Stock solutions of **2** (4 mM in DMF), and 2-aminophenol (10 mM in CH_3CN) were prepared. 3 mL CH_3CN taken in a cuvette to which (30 µL, 10 mM) 2-aminophenol and (4 mM, 7.5 µL) **2** were added. (B) The reaction of 0.05 mM **2** with 0.1 mM 2-aminophenol under constant purging of O_2 in CH_3CN. Inset: The corresponding changes in the absorption at 425 nm over time in seconds. *Reaction condition:* Stock solutions of **2** (4 mM in DMF), and 2-aminophenol (10 mM in CH_3CN) were prepared. 3 mL CH_3CN taken in a cuvette to which 2-aminophenol (30 µL, 10 mM) and **2** (4 mM, 37.5 µL) were added.

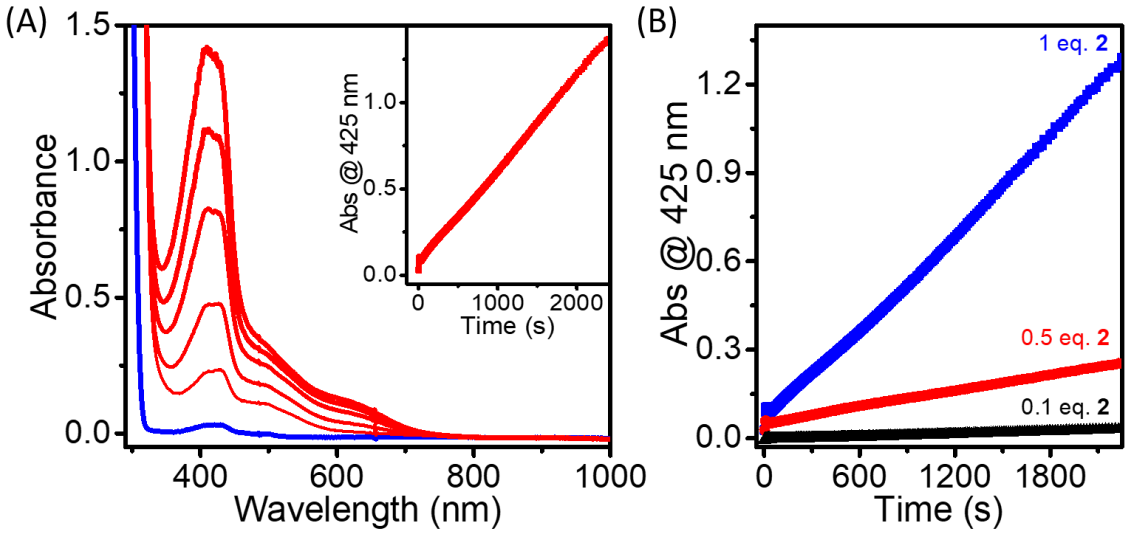

Figure S17. (A) Time-dependent UV-Vis absorption spectral changes upon reaction of 0.1 mM **2** and 0.1 mM 2-aminophenol with purging of O_2 in CH_3CN. Inset: The corresponding changes in the absorption at 425 nm over time in seconds. *Reaction condition:* Stock solutions of **2** (4 mM in DMF), and 2-aminophenol (10 mM in CH_3CN) were prepared. To 3 mL CH_3CN in a cuvette, 2-aminophenol (30 µL, 10 mM) and **2** (4 mM, 75 µL) were added. (B) The changes observed at 425 nm upon adding different equivalents of **2** to 0.1 mM 2-aminophenol (blue) 1 eq. (0.1 mM), (red) 0.5 eq. (0.05 mM) and (black) 0.1 eq. (0.01 mM)

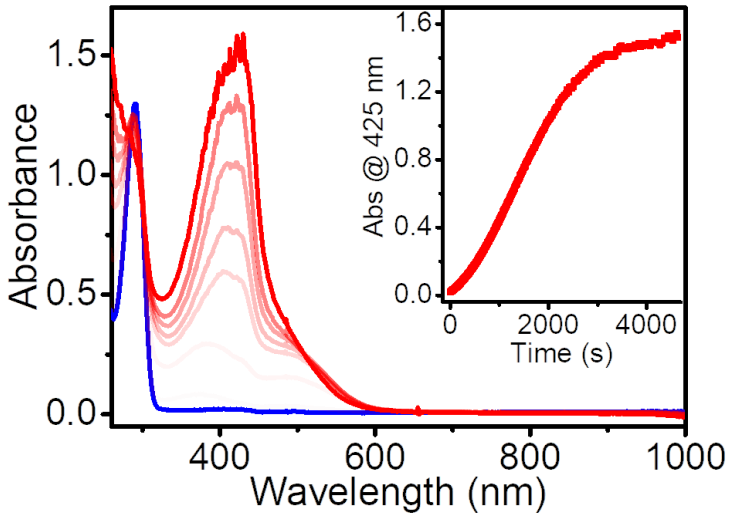

Figure S18: Time-dependent UV-Vis absorption spectral changes upon the reaction of 5 µM **1** and 0.5 mM 2-aminophenol under constant purging of O_2 in CH_3CN at 40 °C. Inset: The corresponding changes in the absorption at 425 nm over time in seconds. *Reaction condition:* Stock solutions of **1** (1 mM in CH_3CN) and 2-aminophenol (100 mM in CH_3CN) were prepared. To a 3 mL CH_3CN in a cuvette, 2-aminophenol (15 µL, 100 mM) and **1** (1 mM, 15 µL) were added.

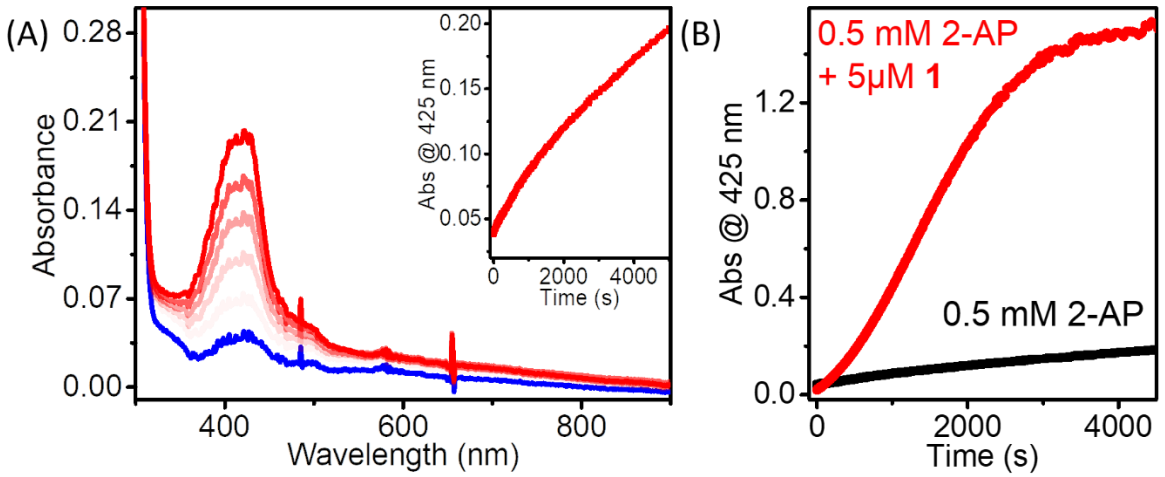

Figure S19: (A) Time-dependent UV-Vis absorption spectral changes upon treating 0.5 mM 2-aminophenol with O_2 (purging) in CH_3CN at 40 °C. Inset: The corresponding changes in the absorption at 425 nm over time in seconds. (B) Time trace at 425 nm for catalytic reaction of 0.5 mM 2-aminophenol with 5 µM **1** (red) and only 0.5 mM 2-aminophenol (black) with purging O_2 in CH_3CN at 40 °C. *Reaction condition:* 2-aminophenol (100 mM in CH_3CN) stock prepared. To a 3 mL CH_3CN in a cuvette 2-aminophenol (15 µL, 100 mM) was added.

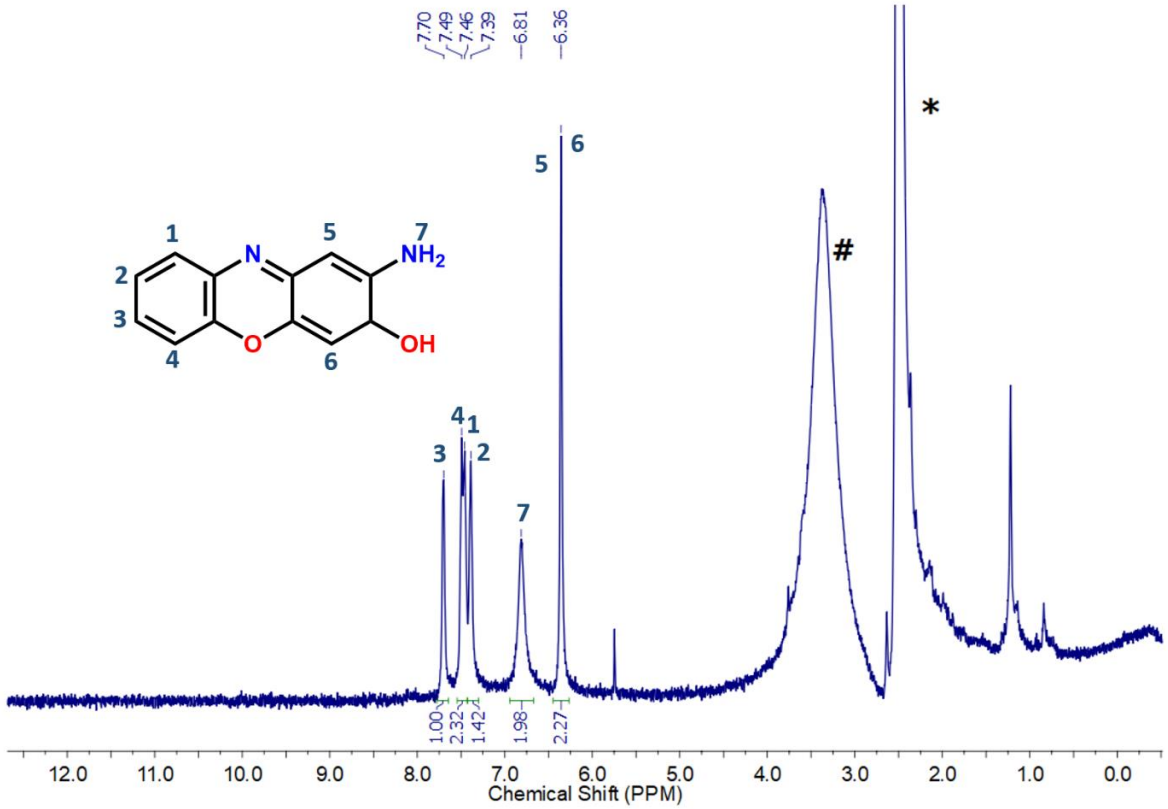

Figure S20: ^1H NMR of 2-amino-3*H*-phenoxazin-3-one. (*DMSO-d6 residual peak, # peak for H_2O in DMSO-d6)

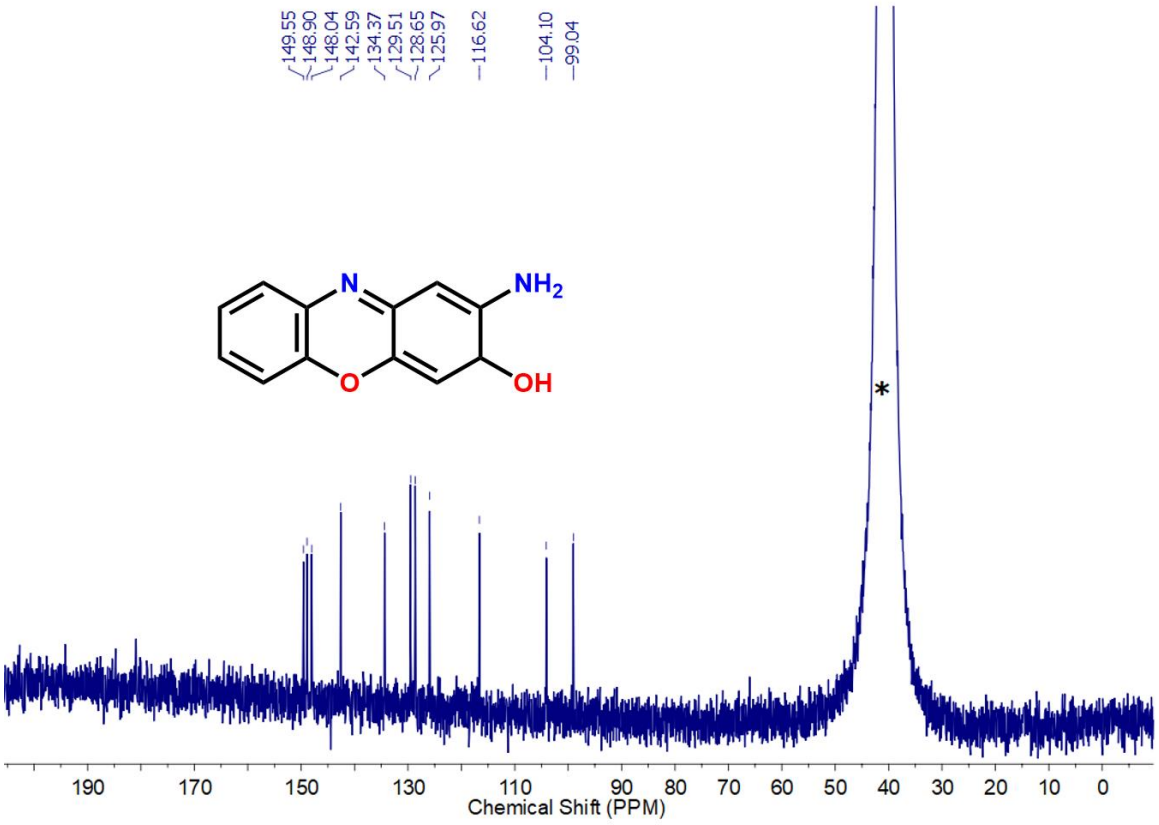

Figure S21: ^{13}C NMR of 2-amino-3*H*-phenoxazin-3-one. (*DMSO-d6 residual peak)

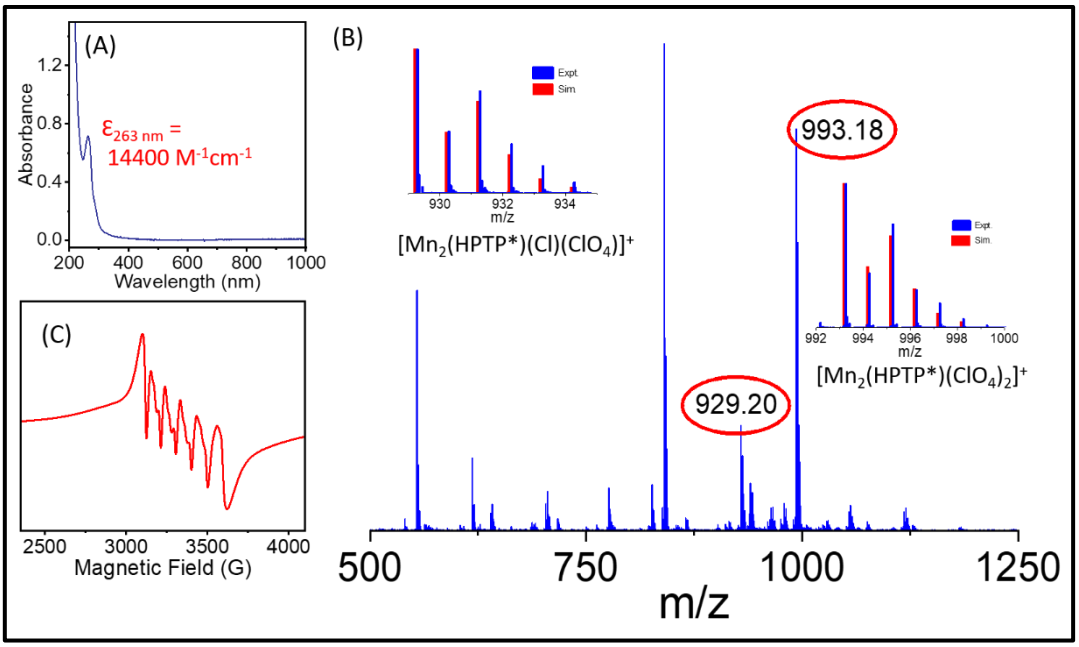

Figure S22: (A) UV-Vis absorption spectrum of 0.05 mM Mn dimer, $[Mn^{II}_2(HPTP^*)]^{3+}$, **3** in CH_3CN. (B) ESI-MS of **3** in CH_3CN. (C) X-band EPR spectrum of **3** in solution state measured in MeOH with a few drops of toluene at 120 K; modulation amplitude 1.98 G, modulation frequency 100 kHz, and microwave frequency 9.466 GHz.

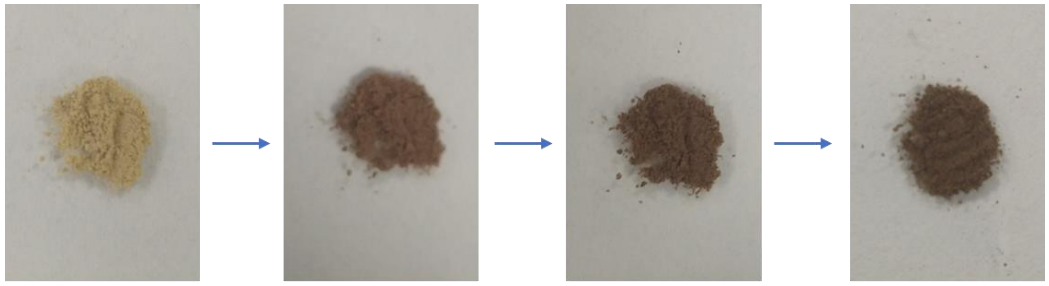

Figure S23: Conversion of Mn_2(II) dimer, $[Mn^{II}_2(HPTP^*)]^{3+}$, (**3**) to **1** upon the exposure to open air.

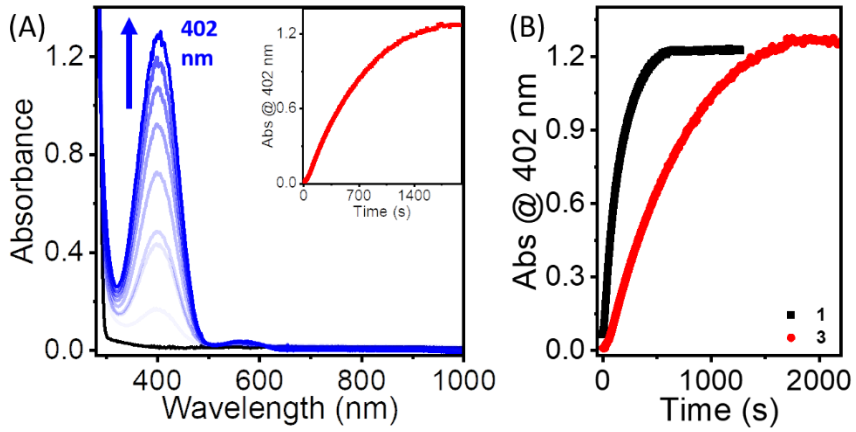

Figure S24: (A) Time-dependent UV-Vis absorption spectral changes upon the reaction of 1 mM 3,5-DTBC with $[Mn^{II}_2(HPTP^*)]^{3+}$, **3** (60 µM) in CH_3CN under aerobic condition. Inset: The corresponding changes in the absorption at 402 nm due to the formation of 3,5-DTBQ over time (in seconds). (B) Comparison of the rate of reaction monitored using 402 nm (due to the formation of 3,5-DTBQ over time) for the reaction of 3,5-DTBC with **1** (black) and $[Mn^{II}_2(HPTP^*)]^{3+}$**, 3** (red).

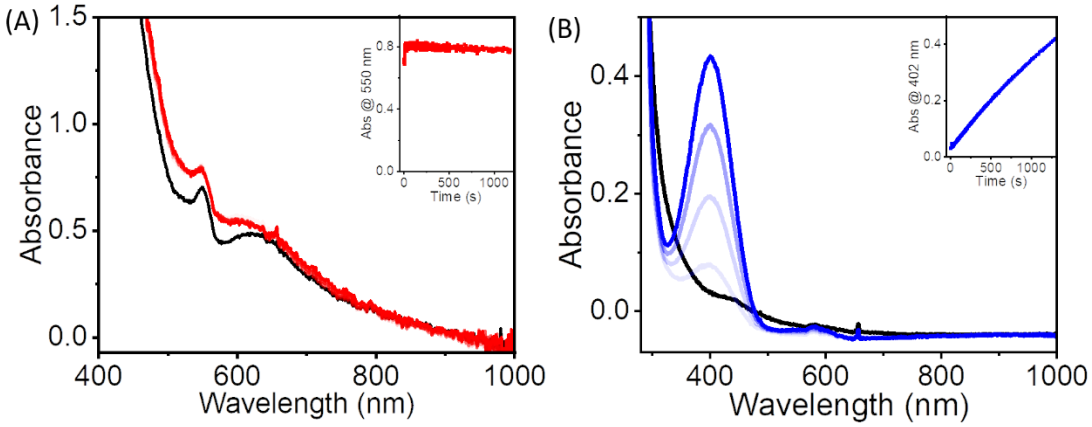

Figure S25: Time-dependent UV-Vis absorption spectral changes upon (A) the reaction of 1.5 mM **1** in CH_3CN with 100 eq. H_2O_2. Inset: The corresponding changes in the absorption at 550 nm over time (in seconds). (B) The reaction of 1 mM 3,5-DTBC with 30 µM **1** in CH_3CN with 5 eq. H_2O_2 under nitrogen atmosphere. Inset: The corresponding changes in the absorption at 402 nm due to the formation of 3,5-DTBQ over time (in seconds).

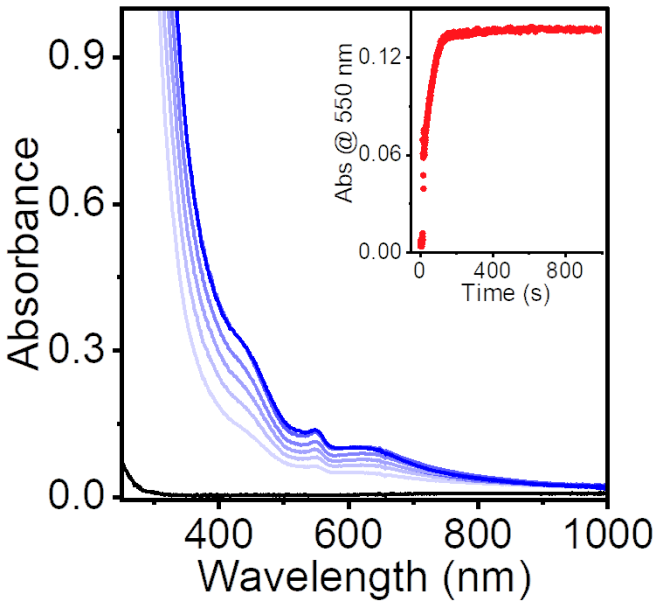

Figure S26: UV/Vis absorption spectral changes observed upon the reaction of 0.5 mM $[Mn^{II}_2(HPTP^*)]^{3+}$, **3** with 5 eq. H_2O_2 under nitrogen atmosphere.

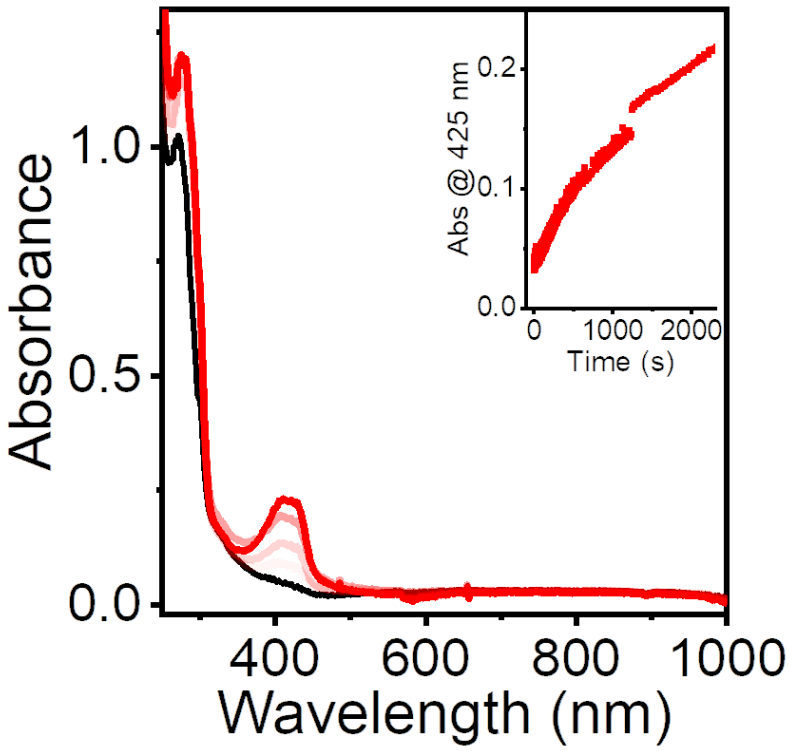

Figure S27: Time-dependent UV-Vis absorption spectral changes upon the reaction of 0.1 mM 2-aminophenol with 10 µM **1** in CH_3CN with 5 eq. H_2O_2 under nitrogen atmosphere. Inset: The corresponding changes in the absorption at 425 nm due to the formation of 2-amino-3*H*-phenoxazin-3-one (APX) over time (in seconds).

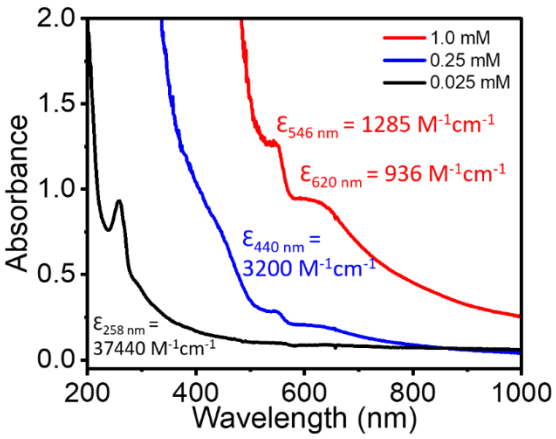

Figure S28: Concentration dependent UV-Vis absorption spectra of $[Mn_4(tpdp)_2(O)_2(H_2O)_4](ClO_4)_5$ (**4**) (where Htpdp = 1,3-bis[bis(2-pyridylmethyl)amino]-2-propanol) (1 mM red, 0.25 mM blue, and 0.025 mM black) in CH_3CN at room temperature.

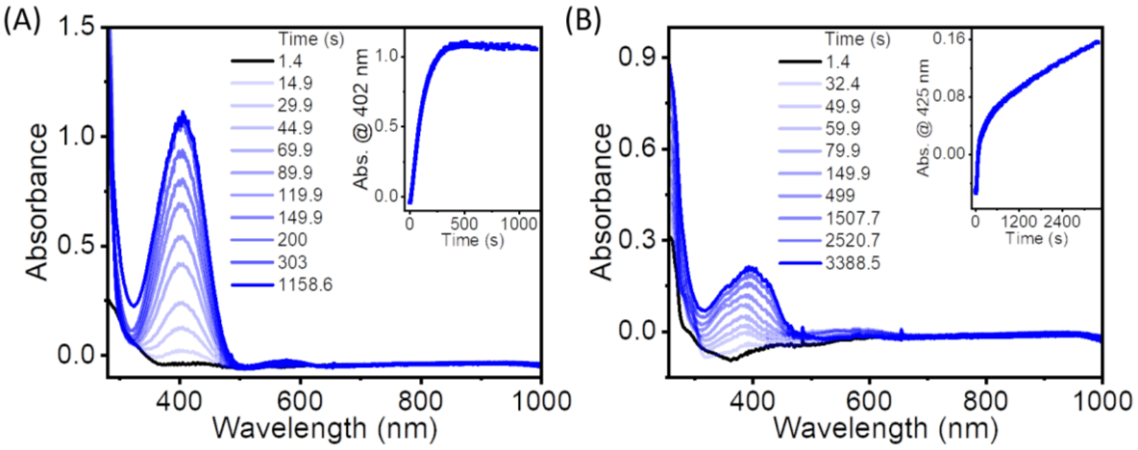

Figure S29: Time-dependent UV-Vis absorption spectral changes upon the reaction of (A) 1 mM 3,5-DTBC with 30 µM $[Mn_4(tpdp)_2(O)_2(H_2O)_4](ClO_4)_5$ (**4**) at room temperature. Inset: The corresponding absorption changes at 402 nm due to 3,5-DTBQ over time. (B) 0.1 mM Aminophenol with 10 µM **4** along with oxygen purging at room temperature. Inset: The corresponding changes in the absorption at 425 nm (due to APX) over time.

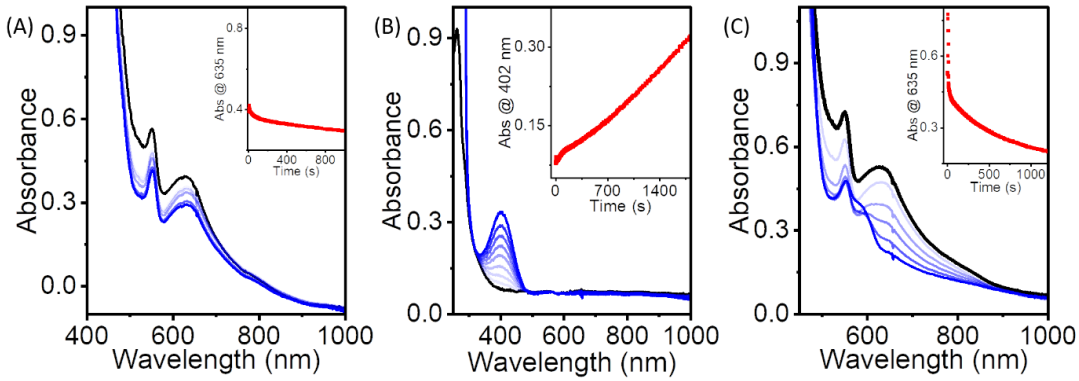

Figure S30: UV/Vis absorption changes upon the reaction of (A) 1.5 mM **1** with 100 eq. 3,5-DTBC at -40 °C. (B) 30 µM **1** with 33 eq. 3,5-DTBC at -20 °C. (C) 1.5 mM **1** with 100 eq. 3,5-DTBC at -20 °C.

Table S1: Crystal data and structure refinement of **1**.

Empirical formula	$C_{78}H_{111}Cl_4Mn_4N_{12}O_{32}$
Formula weight	2090.34
Temperature/K	100(2)
Crystal system	triclinic
Space group	*P-1*
a/Å	11.6386(11)
b/Å	14.8042(14)
c/Å	16.7878(16)
α/°	95.953(2)
β/°	93.623(2)
γ/°	108.608(2)
Volume/*Å*^{3}	2712.3(4)
Z	1
ρ_{calc} g/cm^3	1.280
μ/mm^{-1}	0.628
F(000)	1087.0
Crystal size/mm^3	0.18 × 0.16 × 0.16
Radiation	MoKα (*λ* = 0.71073)
2Θ range for data collection/°	4.606 to 50.094
Index ranges	-13 ≤ h ≤ 13, -17 ≤ k ≤ 17, -19 ≤ l ≤ 19
Reflections collected	38201
Independent reflections	9595 [R_{int} = 0.0528, R_{sigma} = 0.0571]
Data/restraints/parameters	9595/155/616
Goodness-of-fit on F^2	1.020
Final R indexes [I>=2σ (I)]	R_1 = 0.0826, wR_2 = 0.2078
Final R indexes [all data]	R_1 = 0.1172, wR_2 = 0.2406
Largest diff. peak/hole / e Å^{-3}	1.14/-1.45

Table S2: Selected Bond Lengths for **1**.

Atom	Atom	Length/Å		Atom	Atom	Length/Å
Mn1	Mn1[1]	2.7204(15)		Mn2	O6	2.181(4)
Mn1	O6	1.932(4)		Mn2	N6	2.284(4)
Mn1	O5	1.822(4)		Mn2	N4	2.192(3)
Mn1	O5[1]	1.840(4)		Mn2	O7	2.101(5)
Mn1	N5	2.075(4)		Mn2	N3	2.198(4)
Mn1	N2	2.089(2)		Mn2	O8	2.290(6)
Mn1	N1	2.116(4)				

[1]1-X,1-Y,-Z

Table S3: Selected Bond Angles for **1**.

Atom	Atom	Atom	Angle/˚		Atom	Atom	Atom	Angle/˚
O6	Mn1	N5	86.50(17)		O6	Mn2	N6	78.89(16)
O6	Mn1	N2	87.52(14)		O6	Mn2	N4	96.28(13)
O6	Mn1	N1	87.44(17)		O6	Mn2	N3	100.67(16)
O5	Mn1	O6	97.17(17)		O6	Mn2	O8	177.0(2)
O5[1]	Mn1	O6	178.78(17)		N6	Mn2	O8	103.2(2)
O5	Mn1	O5[1]	84.0(2)		N4	Mn2	N6	75.57(13)
O5	Mn1	N5	176.32(19)		N4	Mn2	N3	141.63(15)
O5[1]	Mn1	N5	92.29(18)		N4	Mn2	O8	82.30(18)
O5	Mn1	N2	102.04(14)		O7	Mn2	O6	88.94(19)
O5[1]	Mn1	N2	92.38(15)		O7	Mn2	N6	167.6(2)
O5	Mn1	N1	102.14(16)		O7	Mn2	N4	103.5(2)
O5[1]	Mn1	N1	92.17(17)		O7	Mn2	N3	110.9(2)
N5	Mn1	N2	78.27(15)		O7	Mn2	O8	88.8(3)
N5	Mn1	N1	77.73(17)		N3	Mn2	N6	74.33(15)
N2	Mn1	N1	155.73(16)		N3	Mn2	O8	82.0(2)
Mn1	O6	Mn2	135.68(17)		O5[1]	Mn1	Mn1[1]	41.76(12)
Mn1	O5	Mn1[1]	96.0(2)		O5	Mn1	Mn1[1]	42.28(12)
N2	Mn1	Mn1[1]	99.66(10)		O6	Mn1	Mn1[1]	139.45(12)
N1	Mn1	Mn1[1]	99.58(13)		N5	Mn1	Mn1[1]	134.05(15)

[1]1-X,1-Y,-Z

References:

[1] M. APEX2 (Version **2008**. 6-1), SAINT (V7.60A), SADABS (Version **2008**/1), XPREP (Version 2008/2). (**2005-2009**) Bruker AXS Inc., Madison.

[2] O. V. Dolomanov, L. J. Bourhis, R. J. Gildea, J. A. K. Howard, H. Puschmann, *J. Appl. Cryst.* **2009**, *42*, 339–341.

[3] G. M. Sheldrick, *Acta Cryst.* **2015**, *A71*, 3–8.

[4] G. M. Sheldrick, *Acta Cryst.* **2015**, *C71*, 3–8.

[5] S. Masatatsu, S. Hitoshi, S. Machiko, S. Toshiharu and U. Akira, *Chem. lett.*, 1990, **19**, 923-926.

[6] Y. Mikata, M. Wakamatsu, H. So, Y. Abe, M. Mikuriya, K. Fukui and S. Yano, *Inorg. Chem.*, 2005, **44**, 7268–7270.